ELSEVIER

Journal of Molecular Catalysis A: Chemical 105 (1996) 167–173

JOURNAL OF MOLECULAR CATALYSIS A: CHEMICAL

Study of cumene oxidation over zirconia-, titania- and alumina-based complex oxides obtained by sol–gel methods: activity–structure relationships

Yu.V. Maksimov [a,*], I.P. Suzdalev [a], M.V. Tsodikov [b], V.Ya. Kugel [b], O.V. Bukhtenko [b], E.V. Slivinsky [b], J.A. Navio [c]

[a] *N.N. Semenov Institute of Chemical Physics, Russian Academy of Sciences, Kosygina St., 4, Moscow 117977, Russia*

[b] *A.V. Topchiev Institute of Petrochemical Synthesis, Russian Academy of Sciences, Leninsky Prospect, 29, Moscow 117912, Russia*

[c] *Instituto de Ciencia de Materiales, Universidad de Sevilla – CSIC and Dpto. de Quimica Inorganica, Facultad de Quimica, Sevilla 41012, Spain*

Received 29 January 1995; accepted 15 July 1995

Abstract

Activity–structure relationships have been studied in the low temperature liquid phase cumene oxidation over Fe–O/ZrO_2, Fe–O/TiO_2 and Fe–O/Al_2O_3 complex oxides obtained by sol–gel methods. The study has been carried out by the measurements of overall kinetics, product distribution and by X-ray diffraction and Mössbauer spectroscopic methods. Kinetic study in the presence of homogeneous initiator (azo-bis-diazobutyronitrile) has led to the conclusion that the active surface of complex oxides participates in chain initiation most probably via R–H bond rupture. Three groups of complex oxides are described: (1) two-phase polycrystalline zirconia-based catalysts showing high activity at low iron loading; (2) one-phase polycrystalline zirconia- and titania-based catalysts exhibiting either activity drop at some critical iron content (zirconia) or monotonic activity dependence (titania) on iron loading; (3) amorphous alumina-based catalysts containing γ-ferric oxide clusters and showing monotone activity dependence. Electronically excited terminal Fe=O groups related to the surface FeO_6 polyhedra and iron-containing species located at the interface have been suggested as active centers acquiring the anion-radical behavior. When comparing thermodynamically stable titania (anatase) with metastable one-phase zirconia (cubic or tetragonal) as host matrices, the suggestion was introduced that greater activity of zirconia-based catalysts is due to more energy transfer from the host matrix to the particular active center.

Keywords: Cumene; Oxidation; Zirconia; Titania; Alumina; Sol–gel methods; Activity–structure relationships

1. Introduction

The study of kinetics and mechanism of low temperature cumene oxidation over the surface of simple metal oxides was carried out and discussed in [1–3]. The catalyst surface (S) was suggested to participate in the stages of heterogeneous chain initiation according to the scheme:

$$RH + O_2 + S \rightarrow [RH]_{ads} + [O_2]_{ads} \rightarrow R^{\cdot} + RO_2^{\cdot} \rightarrow \text{Products} \quad (1)$$

while the following reactions (chain propagation, branching and termination) proceed homogene-

* Corresponding author.

Elsevier Science B.V.
SSDI 1381-1169(95)00188-3

ously. The study of structure–activity relationships for Fe–O/Al_2O_3 complex oxides in low temperature hexadecane oxidation has led to the conclusion that active catalysts were composed of substituted γ-alumina and small γ-ferric oxide clusters [4] while the overall rate of hexadecane oxidation increased with an increase in the relative content of magnetic clusters. The electronically excited terminal oxygen of the spinel clusters possessing anion-radical properties was suggested as the active center partaking in free radical generation, most probably via breakage of R–H bonds. Inclusion of nonmagnetic Al^{3+} ions into the γ-ferric oxide lattice reduced the amount of terminal Fe=O groups and overall catalytic activity.

The present work deals with low temperature cumene oxidation over the surfaces of Fe–O/ZrO_2, Fe–O/TiO_2 and Fe–O/Al_2O_3 complex oxides, obtained by sol–gel methods. Overall kinetics and product distribution in the presence of homogeneous initiator (azo-bis-diazobutyronitrile, AIBN) and catalysts were studied in order to elucidate the role of complex oxides in the reaction mechanism. Activity–structure relationships were obtained by kinetic measurements, X-ray diffraction and Mössbauer spectroscopic methods.

2. Experimental

2.1. Initial materials

An oxidizing gas (air) was purified by passing through a molecular sieve trap kept at 77 K. The purification of cumene from peroxides and chemical stabilizers was carried out as described in the recent paper [5]. Chlorobenzene (Aldrich, HPLC, 99.9% purity), was used as the solvent for the oxidation reaction. Acetylacetone, the solvent for synthesis of Fe(acac)$_3$, was subjected to multiple distillation. Homogeneous initiator azo-bis-diazobutyronitrile (96–98% purity, GLC), was carefully purified by successive double recrystallization from ethanol and benzene.

2.2. Catalyst preparation

Fe–O/ZrO_2 (catalysts **I**-1 and **I**-2), Fe–O/TiO_2 (**II**) and Fe–O/Al_2O_3 (**III**) were synthesized by sol–gel methods using either metallocomplexes (**I**-1, **II**, **III**) or inorganic salts (**I**-2). Iron-containing gel-precursors of catalysts **I**-1, **II**, **III** were obtained by hydrolysis of $Zr(O^iPr)_4$, $Ti(O^nBu)_4$ and $Al(O^iPr)_3$ in benzene solution containing different amounts of iron acetylacetonate [6]. Fe(acac)$_3$ was prepared by electrochemical anodic dissolution of metallic Fe in acetylacetone [7]. The ratio Fe(acac)$_3$/M(OR)$_x$ (M = Zr, Ti, Al; x = 3, 4) in gel-precursors was varied in order to obtain samples with different iron loading. Catalysts **I**-1, **II** and **III** were obtained by annealing the gel-precursors at 500°C, 5 h. and contained 0.2, 0.5, 0.7, 1.5, 2.3, 3.2, 7.8 and 11.8 wt.% Fe (**I**-1); 0.5, 1.0, 2.0, 5.0 and 10.0 wt.% Fe (**II**); and 1.0, 2.3, 6.3, 13.6 and 20.0 wt.% Fe (**III**), respectively. Zirconia-based catalysts **I**-2 were prepared by calcination at 500°C, 5 h. of gel-precursors produced by hydrolysis of $ZrOCl_2$ and $Fe(NO_3)_3 \cdot 8H_2O$ [8,9]. Catalysts contained 0.5, 0.7, 1.0 and 5.0 wt.% Fe.

2.3. Catalyst characterization

All synthesized catalysts were dispersed powders with granulometric size 5–50 μ. Elemental analysis of the catalysts was carried out using a Perkin Elmer spectrometer AS-400. The values of specific surface area were obtained by BET measurements with benzene as an absorbate. DRON-314 and Philips PW 1700 devices with filtered CuK_α radiation were used for X-ray diffraction analysis. The average size of microcrystallites was estimated from the half-width of the diffraction peaks using the Scherrer equation [10]. The Mössbauer spectra were recorded on an electrodynamic type of equipment with ^{57}Co in chromium as a source. Isomer shifts (IS) are reported relative to α-Fe at room temperature. The spectra were computer-analyzed using the common fit procedure for a series of Lorentians [4].

2.4. Catalytic experiments

Liquid phase cumene oxidation in the presence of AIBN and complex oxides was carried out at $T = 90 \pm 0.1$°C, atmospheric pressure in a manometric, closed, temperature-controlled gasometric device with a magnetic stirrer. No 'blank' reaction was observed in the absence of initiator or catalyst. The distinctive feature of the device used is thin-walled capillaries ($d_{in} = 0.3$–0.4 mm) as rate controlling measuring elements and capacity compensator whose volume is less than 20 times greater than that of a glass reactor. The O_2 uptake was measured in a calibrated gas burette. Specially purified n-decane was used as manometric liquid. Reaction volume, cumene/oxygen ratio and the amount of powdered catalyst were 6 ml, 1/10 and 0.02 g, respectively. The overall rate of oxygen uptake was evaluated from the slope of second quasi-linear part of the S-like kinetic curve [4]. Each measured rate was the mean value from at least three runs. Other experiments showed that the oxidation rate was independent of the mixing rate. The sensitivity of oxidation rate measurement was $\sim 10^{-7}$ mol/l·s. Kinetic measurements were performed at cumene conversion not exceeding 1–2%.

2.5. Reaction products

The products of the reaction were first separated from chlorobenzene and then analyzed chromatographically on a CHROM-5 thermoprogrammable device supplied with flame-ionization detector and 6% polyethylene glycol sebacinate on zeolite 545 packed in a glass column ($l = 3$ m, $d = 0.3$ mm) [11]. Each analysis was conducted at cumene conversion not less than 10–12%.

3. Results

3.1. Kinetic study

Fig. 1 presents kinetic data of oxygen uptake in the presence of heterogeneous initiators (catalysts I-1, I-2, II and III, containing 5 wt.% Fe) or homogeneous initiator (AIBN). We suggest that the stages of heterogeneous and homogeneous chain initiation proceed by the reactions (1) and

$$\mathrm{AIBN} + \mathrm{RH} \rightarrow \mathrm{R}^{\cdot} \qquad (2)$$

respectively. The stages of chain propagation, branching and termination are realized in the liquid phase, i.e. homogeneously:

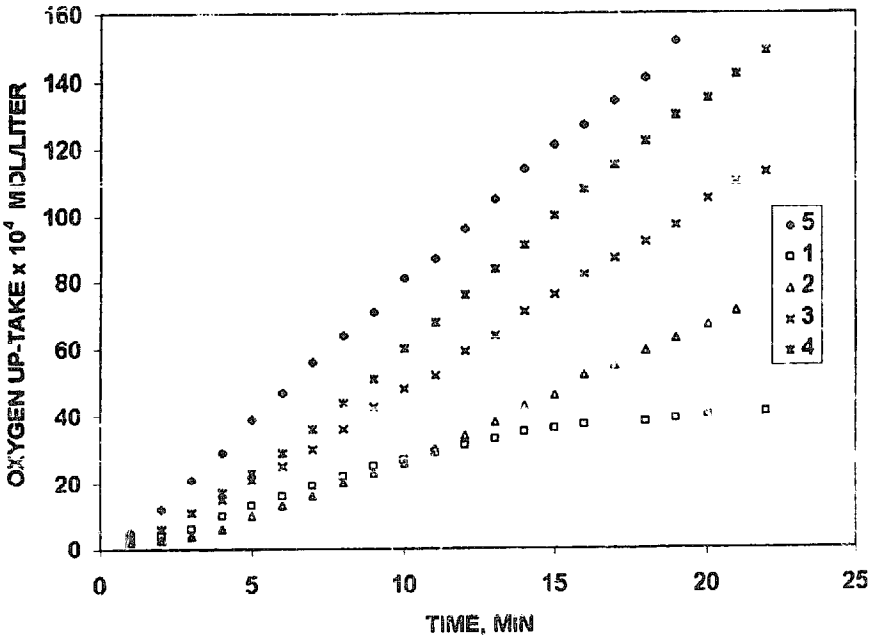

Fig. 1. Kinetic data on cumene oxidation in the presence of heterogeneous initiators–complex oxides (5 wt.% Fe) and homogeneous initiator AIBN ($5 \cdot 10^{-3}$ mol/l) at $T = 90$°C, $P = 0.1$ MPa. (1) Fe–O/TiO_2, (2) Fe–O/ZrO_2 (I-2), (3) Fe–O/ZrO_2 (I-1), (4) Fe–O/Al_2O_3, (5) AIBN.

$$R^{\cdot} + O_2 \rightarrow RO_2^{\cdot} \quad (3)$$

$$RO_2^{\cdot} + RH \rightarrow ROOH + R^{\cdot} \quad (4)$$

$$2RO_2^{\cdot} \rightarrow \text{Products} \quad (5)$$

where RH, $R^{\cdot}$ and $RO_2^{\cdot}$ are hydrocarbon, alkyl and peroxide radicals, respectively. For the chain termination effected by (5), small value of ROOH, high concentration of dissolved oxygen and long chains, the overall oxidation rates in the presence of only catalysts (W_{het}) or AIBN (W_{hom}) are expressed by

$$W_{het} = W_i^{0.5} \cdot k_4 \cdot k_5^{-0.5} \cdot [RH] \quad (6)$$

and

$$W_{hom} = W_i^{0.5} \cdot k_4 \cdot k_5^{-0.5} \cdot [RH] \quad (7)$$

respectively. In the simultaneous presence of catalyst and AIBN the overall rate of oxygen uptake (W_Σ) is expressed by

$$W_\Sigma (W_i + W_2)^{0.5} \cdot k_4 \cdot k_5^{-0.5} \cdot [RH] \quad (8)$$

or

$$W_\Sigma = (W_{hom}^2 + W_{het}^2)^{0.5} \quad (9)$$

The results presented in Table 1 confirm that an active surface of complex oxides participates mainly in chain initiation most probably via R–H bond rupture just as it takes place over an active surface of simple oxides [1–3,5]. The radicals, formed on the catalyst surface, diffuse into the liquid phase and take part in chain propagation, termination, etc. This explanation seems to be borne out by the data on product distribution discussed below.

Table 1
The overall rates of cumene oxidation measured in the presence of heterogeneous initiators–catalysts [a]

Data	AIBN	I-1		I-2		III
		Fe, wt.%		Fe, wt.%		Fe, wt.%
		0.5	5	5	2.3	6.3
W_{hom}	16.2	–	–	–	–	–
W_{het}	–	13.4	10.0	8.3	13.6	13.7
$W_{\Sigma(exp)}$	–	20.0	18.5	20.1	22.0	19.5
$W_{\Sigma(calc)}$	–	21.0	19.0	18.2	21.8	21.9

[a] $Fe-O/ZrO_2$ (I-1, I-2), $Fe-O/Al_2O_3$ (III) ($W_{het} \cdot 10^6$ mol/l·s), homogeneous initiator = AIBN ($W_{hom} \cdot 10^6$ mol/l·s) or in the simultaneous presence of catalyst and AIBN ($W_{\Sigma(exp)} \cdot 10^6$ mol/l·s); $T = 90$ °C, [RH] = 1.2 mol/l, [AIBN] = $5 \cdot 10^{-3}$ mol/l. The values of $W_{(calc)}$ are the overall rates of cumene oxidation calculated by Eq. (10).

3.2. Activity–structure relationships

Table 2 presents the data on iron content, specific surface area (S_{sp}), catalyst structure, overall activity over the crystalline samples (W_{het}) and reduced activity of crystalline samples (A) normalized by total surface area. Independent of preparation, unloaded ZrO_2 is inactive in hydrocarbon oxidation, while surfaces of TiO_2 and Al_2O_3 exhibit small activation. Iron-loaded systems show peculiar behavior.

Consider catalysts I-1. Unloaded polycrystalline ZrO_2 is a heterogeneous composition of tetragonal and monoclinic crystals with unit cell parameters $a = 0.506$ nm, $c = 0.515$ nm and $a = 0.515$ nm, $b = 0.530$ nm, $c = 0.531$ nm, $\theta = 99°\,23'$ respectively, which are close to table values [12]. Loading of 0.2–0.7 wt.% Fe dramatically changes the zirconia structure. Thus, at 0.5 wt.% Fe the catalyst is 90% cubic ($a = 0.508$ nm) and 10% monoclinic. Room temperature Mössbauer spectrum shows a doublet of high-spin octahedral Fe^{3+} sites (IS = 0.37 ± 0.03 mm/s, QS = 1.00 ± 0.03 mm/s and $\Gamma \approx 0.75$ mm/s), in which significant line broadening indicates the dispersion in local electronic parameters. Thus, a small amount of iron facilitates cubic phase formation but the zirconia-based catalyst is still heterogeneous. The high catalytic ability of the sample seems to be due to the presence of iron-containing specimens (e.g. distorted FeO_6 polyhedra) located in the vicinity of the interface.

Inclusion of 1.5 and 2.3 wt.% Fe causes the striking effect of one-phase cubic zirconia formation with mean values of unit cell parameter and crystal size $\langle a \rangle = 0.507$ nm and $\langle d \rangle = 23$–25 nm, respectively. Mössbauer data indicate that the ferric ion (IS = 0.36 ± 0.03 mm/s, QS = 0.98 ± 0.03 mm/s and $\Gamma \approx 0.55$ mm/s) is

Table 2
Iron content, specific surface area (S_{sp}), structure, overall (W_{het}) and reduced activity (A) of Fe–O/ZrO_2 (I-1, I-2), Fe–O/TiO_2 (II) and Fe–O/Al_2O_3 (III) catalysts in cumene oxidation

Catalyst	Iron content wt.%	S_{sp} m^2/g	Structure	Experimental rate $W_{het} \cdot 10^6$ mol/l·s	A [a]
FeO/ZrO_2 (I-1)	0	24	tetragon. monocl.	0	0
	0.2	24	cubic 0.4 monocl. 0.6	7.3	0.54
	0.5	24	cubic 0.9 monocl. 0.1	13.4	1
	0.7	24	cubic 0.95 monocl. 0.05	9.2	0.69
	1.5	24	cubic	0	0
	2.3	24	cubic	0	0
	3.1	24	cubic	5.6	0.42
	5.0	22	cubic	10.0	0.82
	7.0	20	cubic	9.4	0.84
	11.7	18	amorph.	5.0	–
FeO/ZrO_2 (I-2)	0	15	monocl. tetragon.	0	0
	0.5	15	monocl. 0.7 tetragon. 0.3	7.3	1.1
	0.7	15	monocl. 0.7 tetragon. 0.3	6.1	0.9
	1.0	15	tetragon.	0	0
	5.0	15	tetragon.	8.3	0.9
FeO/TiO_2	0	64	tetragon.	2.6	0.07
	0.5	64	tetragon.	2.9	0.08
	1.0	64	tetragon.	3.1	0.09
	2.0	64	tetragon.	4.7	0.13
	5.0	60	tetragon.	6.5	0.19
	10.0	55	tetragon.	6.0	0.20
FeO/Al_2O_3	0	300	γ-Al_2O_3	1.7	0.01
	1.0	300	amorph.	6.6	–
	2.3	300	amorph.	13.6	–
	6.3	295	amorph.	13.7	–
	13.6	290	amorph.	14.2	–
	20.0	285	amorph.	14.5	>1 [a]

[a] Overall activity normalized by total surface area, in relative units.
[b] Estimated value (see text).

characterized by narrower distribution in local electronic parameters compared to the samples with 0.2–0.7 wt.% of iron loading. The catalysts are inactive in cumene oxidation. This fact may be explained that Zr^{4+} ions are substituted by Fe^{3+} ions in pre-surface layers. Iron ions do not occupy surface positions. At further iron loading zirconia-based catalysts remain cubic but show ever growing crystallinity loss. Thus, at 5 wt.% Fe the value of the mean crystal size is $\langle d \rangle \approx 9$–10 nm. The indexes W_{het} increase, reaching maximum values at 5–7 wt.% Fe. Preliminary EXAFS data suggest that iron ions occupy surface positions at the edges of zirconia crystallites restricting their growth [6].

At maximum iron loading (Fe = 11.7 wt.%) zirconia-based catalyst I-1 becomes X-ray amorphous and overall activity decreases. According to magnetic data [6], the catalyst contains magnetic clusters. Thus, if one compares activity of this sample with that of other catalysts I-1, one should normalize an overall activity not by total surface area but the area of ferric oxide clusters [4].

Except for similarity between catalysts I-1 and I-2 (heterogeneity, concentration dependence of activity, etc.) the difference in phase composition is of significance. Initial sample I-2 is mainly monoclinic ($a = 0.515$ nm, $b = 0.520$ nm, $c = 0.532$ nm, $\theta = 99° 23'$) and contains a small amount of tetragonal structure. Introduction of 0.5–0.7 wt.% Fe causes 70% monoclinic and 30% tetragonal ($a = 0.509$ nm, $c = 0.518$ nm) phase composition. This is accompanied by a significant activity increase. Octahedral complex of high-spin Fe^{3+} shows parameters IS = 0.39 ± 0.03 mm/s, QS = 0.58 ± 0.03 and $\Gamma \approx 0.78$ mm/s. At some critical iron loading (ca. 1.0 wt.% Fe) zirconia becomes one-phase, tetragonal ($a = 0.509$ nm, $c = 0.518$ nm) and completely inactive. Two FeO_6 polyhedra with parameters of high-spin Fe^{3+} IS(1) = 0.34 ± 0.03 mm/s, QS(1) = 0.68 ± 0.03 mm/s, $\Gamma(1) = 0.50 \pm 0.03$ mm/s and IS(2) = 0.35 ± 0.03 mm/s, QS(2) = 1.10 ± 0.03 mm/s, $\Gamma(2) = 0.48 \pm 0.03$ mm/s have relative content 71% and 29%, respectively. Further iron loading preserves the tetragonal structure while activity successively

increases. Parameters of unique FeO_6 take values IS = 0.38 ± 0.03 mm/s, QS = 1.01 ± 0.03 mm/s and Γ = 0.46 ± 0.03 mm/s.

Unloaded TiO_2 possesses tetragonal structure (anatase, a = 0.376 nm, c = 0.944 nm) and exhibits a small oxidation rate. The indexes W_{het} steadily increase with iron loading reaching a plateau at ~5 wt.% Fe. Each iron-containing sample preserves the anatase structure and contains two FeO_6 polyhedra of high spin Fe^{3+} (IS(1) = 0.35 ± 0.03 mm/s, QS(1) = 0.85 ± 0.03 mm/s, Γ(1) = 0.48 ± 0.03 mm/s and IS(2) = 0.34 ± 0.03 mm/s, QS(2) = 1.10 ± 0.03 mm/s, Γ(2) = 0.48 ± 0.03 mm/s) with relative content 45% and 55%, respectively. As in zirconia-based samples, the mean crystal size of titania-based catalysts decreases with iron loading. In fact, samples with 0.5 and 10 wt.% Fe show mean crystal size $\langle d \rangle \approx$ 15–20 nm and 7–9 nm, respectively. One can see from Table 2 that normalized activities of titania-based catalysts, calculated per total surface area, are 3–4 times smaller than that of zirconia-based samples. This fact indicates surface and structure sensitivity of the reaction of liquid phase cumene oxidation. It should be noted that according to magnetic susceptibility measurements taken at 77–300 K, all crystalline catalysts exhibit 'paramagnetic' behavior obeying the Curie–Weiss law with a negative Weiss constant, θ, which absolute indexes increase with iron loading [4,6]. Thus, activity of crystalline complex oxides may be connected with 'paramagnetic' Fe^{3+} sites entering surface or pre-surface layers and forming, most probably, dimers and trimers with dipole–dipole exchange interaction. However, ferric ions seem still to be not involved in magnetic superexchange interaction.

Although amorphous γ-Al_2O_3 possesses negligible activity, X-ray amorphous FeO/Al_2O_3 catalysts, composed of spinel, $Fe_xAl_{2-x}O_3$, and small γ-ferric oxide clusters [4], show considerable activity with W_{het} reaching a plateau at about 3–5 wt.% Fe. The estimation of normalized activity of the sample with 20 wt.% Fe and total surface area of magnetic clusters $S \approx$ 20–30 m^2/g [4] gives $A > 1$, which is one of the highest value (Table 2).

Table 3
Product distribution in liquid phase cumene oxidation

Initiator,	Reaction products, relative units (±1%)		
catalyst	RCOR' [a]	RCOH [a]	RCOOH [a]
AIBN	28	51	13
$Fe-O/ZrO_2$ (I-2)	28	60	10
$Fe-O/TiO_2$	20	65	4
$Fe-O/Al_2O_3$	28	57	5

T = 90 C; cumene conversion 10–12%, Fe = 5 wt.%.
[a] RCOR' = acetophenone; RCOH = phenyl carbinol; RCOOH = cumene hydroperoxide. Other products result from complete oxidation.

Table 3 presents typical data on product distribution. One can see, that main reaction products are the same in the presence of AIBN and over catalyst surfaces. The significant decrease in the relative content of cumene hydroperoxide and corresponding increase in phenylcarbinol yield, which occur over catalyst surface, may indicate the decomposition of cumene hydroperoxide involving homolytic scission of an oxygen to hydrogen bond. Thus, the overall mechanism of the reaction of liquid phase cumene oxidation does include homogeneous–heterogeneous stages.

4. Discussion

Experimental results clearly indicate that the catalytic ability of complex oxides in liquid phase cumene oxidation is determined by the presence of iron-containing surface centers. One can suggest and discuss at least two types of surface active centers related to FeO_6 polyhedron. The first active center is an oxygen of a terminal Fe=O group acquiring anion-radical behavior upon electronic excitation. In fact, the high probability for radiationless transitions in MeO_6 polyhedra of complex oxides (where Me = Cr, V, Fe, Co, etc.) [4,13–15] is due to intersection of potential curves for ground and lowest excited states. That makes it possible to suggest the reversed process of 'back donation'; i.e. lattice-induced electron

excitation of a definite surface group. Electronic excitation of terminal oxygen may be treated as a 'thermal' exchange process deriving from energy transfer from the lattice to the particular Fe=O surface group. The shift in the electron density from O^{2-} to Fe^{3+}, because of excitation, ensures the anion-radical property of surface oxygen. The second active center is interfacial defects of catalyst structure connected to the iron-containing specimens which are responsible for the high activity of Fe–O/ZrO_2 system at low iron loading (~0.5 wt.% Fe). Terminal Fe=O groups seem to play an important role in iron-containing one-phase zirconia and titania catalysts. The fact that metastable zirconia (cubic or tetragonal) carrying an excess of lattice energy shows greater catalytic ability than thermodynamically stable titania (anatase), seems to testify to more energy transfer from ZrO_2 host matrix to a specific Fe=O group. This phenomenon demonstrates the effect of the (Fe–O)-support interaction.

The participation of both centers in heterogeneous activation may be expressed by the following scheme:

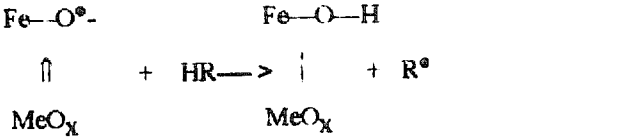

(11)

with the stage of active center regeneration as:

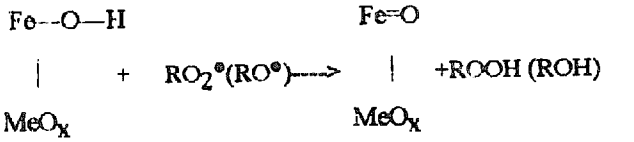

(12)

As to decomposition of cumene hydroperoxide over the catalyst surface (Table 3), it may take place on an active center [16]:

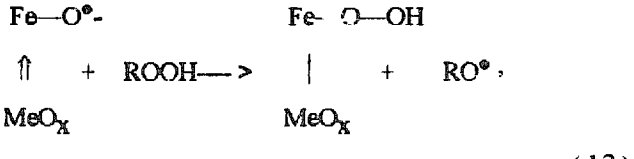

(13)

followed by chain propagation:

$$RO^{\cdot} + RH \rightarrow ROH + R \quad (14)$$

Thus, iron-containing zirconia-, titania- and alumina-based complex oxides, obtained by sol–gel methods, show considerable activity and structure sensitivity in liquid phase cumene oxidation. Therefore this reaction can be used as a sensitive tool to study the peculiarities of complex oxide structure.

Acknowledgements

The authors thank the Russian Science Foundation (Project 94-03-08081), International Science Foundation (Grant MOI000) and NATO High Technology Foundation (HTECH.CRG 931258) for financial support of this work.

References

[1] H.W. Melville and S. Richards, J. Chem. Soc., 3 (1954) 944.
[2] H. Hock and H. Kropf, Z. Frakt. Chem., 9 (1959) 173.
[3] N.M. Emanuel (Ed.), Teoria i Practica Gidrophaznogo Okyslenia, Nauka, Moskva, 1974, p. 330.
[4] M.V. Tsodikov, V.Ya. Kugel, Yu.V. Maksimov, O.G. Ellert, V.M. Shcherbakov and O.V. Bukhtenko, J. Catal., 148 (1994) 113.
[5] M.V. Tsodikov, V.Ya. Kugel, Yu.V. Maksimov, T.N. Zdanova, A.E. Shlikhter, T.S. Vinogradova and D.I. Kochubey, Petrochemistry, 34 (1994) 202.
[6] M.V. Tsodikov, O.G. Ellert, D.I. Kochubey, O.V. Bukhtenko and V.M. Shcherbakov, J. Mater. Sci., 30 (1995) 1087.
[7] V.A. Shreider, E.P. Turevskaya, N.I. Kozlova and N.Ya. Turova, Inorg. Chim. Acta, 53 (1981) L73.
[8] J.A. Navio, M. Macias and P.J. Sanches-Soto, J. Mater. Sci. Lett., 11 (1992) 570.
[9] J.A. Navio, F.J. Marchena, M. Macias, P.J. Sanches-Soto and P. Pichat, J. Mater. Sci., 27 (1992) 2463.
[10] S.S. Gorelik, L.N. Rastorguev and Yu.A. Shakov, Rentgenographicheskii i Electronographicheskii Analysis, Metallurgi, Moscow, 1970, p. 450.
[11] N.D. Cheronis and T.S. Ma, Organic Functional Group Analysis by Micro and Semimicro Methods, John Wiley and Sons, New York, 1964.
[12] ASTM, card nos. 14-534; 13-307; 7-337.
[13] A.H. Gritscov, V.A. Shvets and V.B. Kazansky, Chem. Phys Lett., 35 (1075) 511.
[14] V.B. Kazansky, in G.C. Bond, P.B. Wells and F.C. Tompkins (Eds), Proceedings of the 6th International Congress on Catalysis, London, 1976, 1, p. 50.
[15] Yu.V. Maksimov and V.V. Gustov, Chim. Vysokich. Energ., 14 (1980) 505.
[16] Yu.D. Norikov and E.L. Blumberg, Probl. Kinet. Katal. (Moscow), 16 (1975) 150.